Delft University of Technology

Focused vibrotactile stimuli from a wearable sparse array of actuators

de Vlam, Valerie; Wiertlewski, Michael; Vardar, Yasemin

Important note
To cite this publication, please use the final published version (if applicable).
Please check the document version above.

Focused Vibrotactile Stimuli From a Wearable Sparse Array of Actuators

Valerie de Vlam, Michaël Wiertlewski ⓘ, *Member, IEEE*, and Yasemin Vardar ⓘ, *Member, IEEE*

Abstract—Wearable vibrotactile actuators are non-intrusive and inexpensive means to provide haptic feedback directly to the user's skin. Complex spatiotemporal stimuli can be achieved by combining multiple of these actuators, using the funneling illusion. This illusion can funnel the sensation to a particular position between the actuators, thereby creating virtual actuators. However, using the funneling illusion to create virtual actuation points is not robust and leads to sensations that are difficult to locate. We postulate that poor localization can be improved by considering the dispersion and attenuation of the wave propagation on the skin. We used the inverse filter technique to compute the delays and amplification of each frequency to correct the distortion and create sharp sensations that are easier to detect. We developed a wearable device stimulating the volar surface of the forearm composed of four independently controlled actuators. A psychophysical study involving twenty participants showed that the focused sensation improves confidence in the localization by 20% compared to the non-corrected funneling illusion. We anticipate our results to improve the control of wearable vibrotactile devices used for emotional touch or tactile communication.

Index Terms—Haptic interfaces, skin mechanics, tactile perception, wearable technology.

I. INTRODUCTION

RECENT advances in human-robot interaction [1] teler-obotics [2], and virtual reality [3] have demonstrated that haptic feedback can enhance user experience and task performance. In particular, wearable haptic devices have received significant attention for their ease of use and effective utilization for various applications, such as communication, health, and entertainment. The ideal wearable haptic device should be lightweight, easy to wear, and compact [4]. Moreover, as most wearable devices convey haptic feedback through passive touch, naturalistic stimuli require activating an array of actuators simulating movement or generating localized stimuli at multiple sites- requiring high spatial resolution and precision. However, embedding a collection of actuators on the fingertips or other body parts is challenging due to size, weight, and control constraints.

One promising technique for improving spatial resolution without increasing the number of actuators is to leverage the funneling illusion. This illusion, first reported by von Bekesy, is described as perceiving an *illusionary* focused stimulus on a location between two skin sites actuated via vibrotactile stimuli [5]. Over the years, different studies demonstrated the validity of this effect on various body parts, such as fingertips [6], palm, head [7] and even out of the body by funneling between two hands [8], [9]. Altering the amplitude and time delay of the input signal to the actuators, one could control the location of the illusionary stimulus and even create a dynamic motion effect [5], [10]. Recent works also proved the feasibility of this illusion for 2D actuator arrays [8], [11]. Due to its ease of use and effectiveness, funneling illusion is used for many wearable and holdable haptic devices to create exciting virtual experiences [12], [13], [14].

Despite its potential, creating a sharp localized sensation via funneling illusion is not straightforward. The generated illusionary stimulus is usually perceived as distributed in an area whose focal point is hard to localize by the participants [5], [10], [15]. Barghout et al. [15] showed that the average detection rate for localizing the illusionary stimulus generated by two actuators placed on the forearm could be as low as 12%. Although earlier research [16], [17] illustrated that the funneling illusion is encoded centrally in the primary somatosensory cortex, there is also evidence that localization performance can be improved peripherally. The input signal amplitude and frequency, the actuator distance and location, and actuation direction influence the size and intensity of the perceived illusionary stimulus [5], [8], [10]. Previous work [5], [10], [15] explained the reasoning behind these peripheral effects by the wave propagation in the skin; they suggested using skin-stabilizing plates, adhesive tapes, or tangential stimuli to control the transmitted vibrations.

In this study, we investigate whether the perceived localization of a stimulus created by funneling illusion on the arm can be peripherally enhanced by focusing the acoustic waves using the inverse filter technique. This technique has been recently proposed for creating a spatially localized sensation on a flat glass surface by controlling the propagated vibrations [18]. The concept starts with calibrating the propagation medium by finding all the transfer functions that map the dynamic behavior of every actuator to the dynamic behavior of each control point on the surface. This calibration matrix captures the dispersion and attenuation of the vibrating medium and can then be inversed
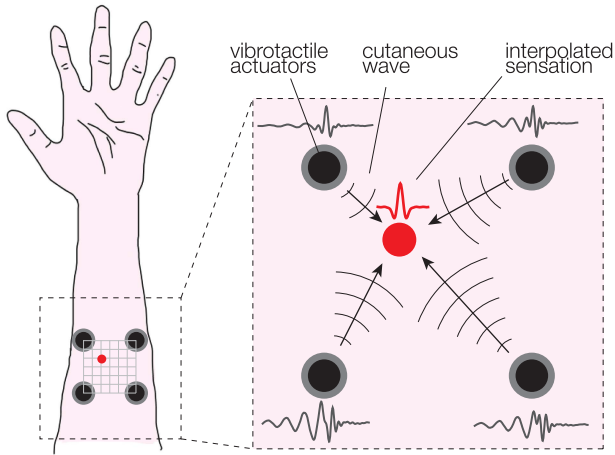
Fig. 1. Cutaneous wave focusing. The harmonic contents of the signal sent to each actuator are delayed and amplified to take into consideration wave propagation and attenuation. A sharp wavelet is felt at the focus point where the waves collapse in space and time.
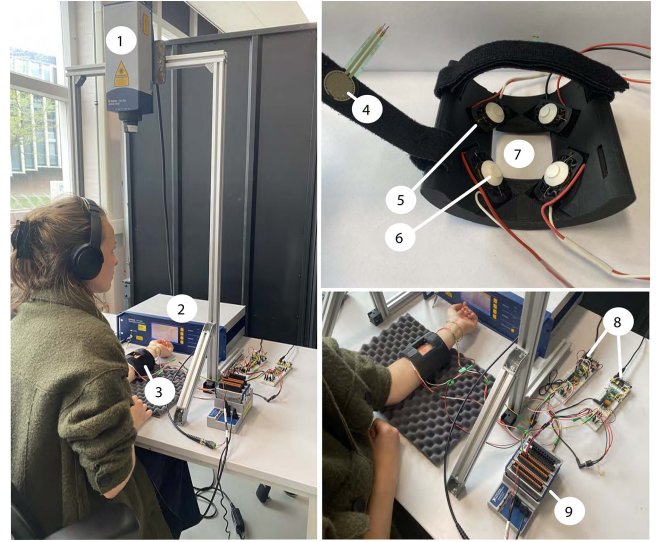

Fig. 2. Experimental setup. It includes a laser doppler vibrometer with a sensor head (1) and controller (2) and the custom-designed wearable device (3), which consists of a force sensor (4), four voice-coil actuators (5) and closed-end cones (6), a square-shaped opening for skin-response measurements (7), voltage amplifiers (8), and a data acquisition board (9).

to compute the signal that needs to be sent to the actuators to generate a specific acoustic pattern on the surface see Fig. 1. For the first time, we apply this technique to focus vibrotactile stimuli directly on the skin.

We developed a wearable device stimulating the volar surface of the forearm composed of four independently controlled actuators. Then, we tested the localization performance and confidence of twenty human participants when focused virtual stimuli at a target location were created by three different techniques: classic funneling illusion, inverse filter, and combination. In the combination method, we used the same principle of inverse filter but targeted the same skin displacement that occurred during the classic funneling illusion for the desired location. We show that the inverse filter provides sharper stimuli that are easier to localize.

II. METHODS

A. Participants

Twenty healthy adults (9 male, 11 female) aged between 19 and 42 years (mean = 25.8, standard deviation = 4.3) participated in the experiments. None of them reported any abnormalities in their tactile or kinesthetic sensory systems. The experimental procedures were conducted in accordance with the Declaration of Helsinki and approved by the Human Research Ethics Committee of TU Delft with case number 1985. All participants gave informed consent.

B. Apparatus

During the experiments, the participants sat on a chair and laid their lower left arms on a foam pad placed on a table (see Fig. 2). They wore a custom-designed tactile device that consisted of a two-by-two array of voice-coil actuators (Tectonic, TEAX14C02-8) placed on the volar surface of their arm. The actuators were spaced by 45 mm between their center points

in both vertical and horizontal directions using a 3D-printed case. The wires connecting the actuators had silicon outer shells, making them very soft and limiting the propagation of acoustic energy. To better ensure vibration distribution, small 3D-printed closed-end cones were attached to the actuators' side in contact with the skin. These cones prevented direct skin contact with the rest of the case, reducing the perceptual masking caused by the undesired propagated vibrations on the casing [19]. The case was attached to the left forearm of the participant via two velcro straps. Two force sensors (FSR, 402) mounted on each strap ensured equal fastening force among the participants. The input voltage signals sent for the actuators were designed through a laptop computer using a graphical user interface programmed using Matlab software, generated via a data acquisition board (NI, cDAQ-9174), and augmented by a power amplifier (MIKROE-3077) with 20 dB gain. The case had a square-shaped opening to allow the measurement of the vibration-induced skin response via a laser doppler vibrometer (Polytec, OFV-505 sensor head, and OFV-5000 controller). Participants wore noise-canceling headphones.

C. Stimuli

1) Base Stimulus: In this study, we strived to create a focused vibrotactile stimulus in time and space. While the focus in space was achieved by either the funneling illusion or the inverse filter, the focus in time was obtained by using a Ricker wavelet which has the form:

$$s(t) = (1 - t^2/\sigma^2)e^{-t^2/\sigma^2} \qquad (1)$$

where t is the time variable and σ is the spread of the wavelet, which was selected as 1 ms in our study. This particular wavelet produces the feeling of a unique tap.

2) Funneling Illusion: When two or more nearby actuators are driven with the same signal, the funneling illusion occurs and creates the sensation that the stimulation originates from a virtual actuator placed in the midpoint of all the actuators [20]. In this scenario, every actuator plays the same base signal $s(t)$ at different scaling factor such that each actuator q produce a signal:

$$s_q(t) = A_q s(t) \tag{2}$$

The scaling factor A_q can be linearly or logarithmically related to the distance between the specific actuator q and the position of the illusory sensation. Seo and Choi reported that the logarithmic approach works better when estimating the intensity of the illusion, while the linear approach is preferred when predicting the location of the illusion [21]. Because our aim is to test stimuli localization, we selected the linear rendering algorithm. The scaling factor was therefore computed as follows [8]:

$$A_q = A \left(1 - \frac{d_q^x}{D^x}\right) \left(1 - \frac{d_q^y}{D^y}\right). \tag{3}$$

Here, A is the maximum driving voltage for the actuators (10 V in our study - after amplification), d_q^x and d_q^y are the horizontal and vertical distances from the actuator q to the virtual actuator location, and D^x and D^y are the maximum distances between the actuators. Once the scaling factor A_q for every actuator was computed, the driving signal for each actuator $s_q(t)$ was determined.

3) Inverse Filter: We used the inverse filter to take into account the delay and attenuation of each frequency due to the propagation and diffusion of acoustic waves in the skin. This technique has its root in medical imaging [22] and has recently been applied to haptics to control multitouch vibrotactile devices [18], [23].

The method starts with a calibration phase, see Fig. 3(a), to build a transfer-function matrix that captures the complex transfer function between every pair of actuators and control points. These transfer functions are defined in the Fourier domain, where the response at each frequency is defined by a single complex number.

The relationship between a signal $s_m(t)$ driving the actuator m and the displacement $u_n(t)$ at a point n on the skin is:

$$u_n(t) = h_{mn}(t) \otimes s_m(t) \tag{4}$$

which in the Fourier domain translates to: $U_n(\omega) = H_{mn}(\omega) S_m(\omega)$ where U, H and S are the Fourier transform of u, h and s respectively.

To calibrate the system, we sequentially excited each actuator with a sine-swept signal from 10 to 1000 Hz and measured the response at every location on the skin. We then computed the Fourier transform of each signal and divided the skin displacement by the actuator signal to find the complex transfer function, $H_{mn}(\omega)$. This calibration phase was conducted with each participant, as their skin properties varied; refer to Section II-D for more details on the procedure.

Once the response of all the points to all the actuators was found we assembled the matrix $\mathbf{H}$ connecting the response of
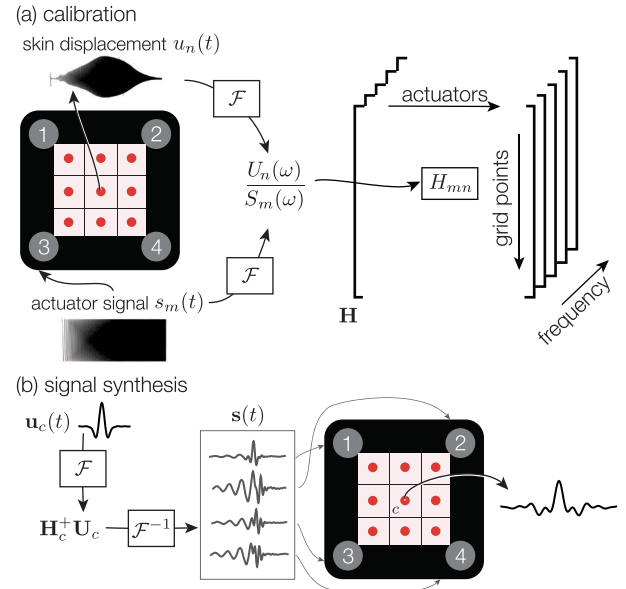

Fig. 3. Signal processing involved in computing the inverse filter. (a) We build a matrix of transfer functions by measuring the response of each point n to each actuator m. (b) Once the calibration matrix is captured, we can inverse it to find the actuator signal that will lead to a specific displacement $s_c(t)$ at the control location c.

all actuators to the movement of all the points:

$$\begin{pmatrix} U_1 \\ U_2 \\ \vdots \\ U_m \end{pmatrix} = \begin{pmatrix} H_{11} & H_{12} & \cdots & H_{1n} \\ H_{21} & H_{22} & \cdots & H_{2n} \\ \vdots & \vdots & \ddots & \vdots \\ H_{m1} & H_{m2} & \cdots & H_{mn} \end{pmatrix} \begin{pmatrix} S_1 \\ S_2 \\ \vdots \\ S_n \end{pmatrix} \tag{5}$$

or

$$\mathbf{U}(\omega) = \mathbf{H}(\omega)\,\mathbf{S}(\omega) \tag{6}$$

Once this matrix was known, it was possible to invert the system to find the actuator signals that could produce a given displacement vector $\mathbf{u}_c(t)$ at given points c. Since the number of control points was different from the number of actuators, the pseudo-inverse was used to find the proper actuator signal such that:

$$\mathbf{S} = \mathbf{H}_c^+ \mathbf{U}_c \tag{7}$$

where $\mathbf{U}_c$ is the Fourier transform of $\mathbf{u}_c$ and $\mathbf{H}_c^+$ is the pseudo inverse of $\mathbf{H}$ where only the c columns are selected.

The time-domain signals to be sent to the actuators are then found by taking the inverse Fourier transform of $\mathbf{S}$. To ensure the algorithm does not lead to large amplitudes near the actuators, in this study, we added four control points placed in the vicinity of the actuators set to zero amplitude in addition to the target displacement. When inverting the system, the control points set to zeros force a solution where the actuators have a moderate amplitude. For the target displacement, $\mathbf{u}_c(t)$, we used our base stimulus, $s(t)$, with a scaling factor of 0.002 mm. This value was selected via preliminary experiments conducted with one actuator and was approximately equal to the peak displacement
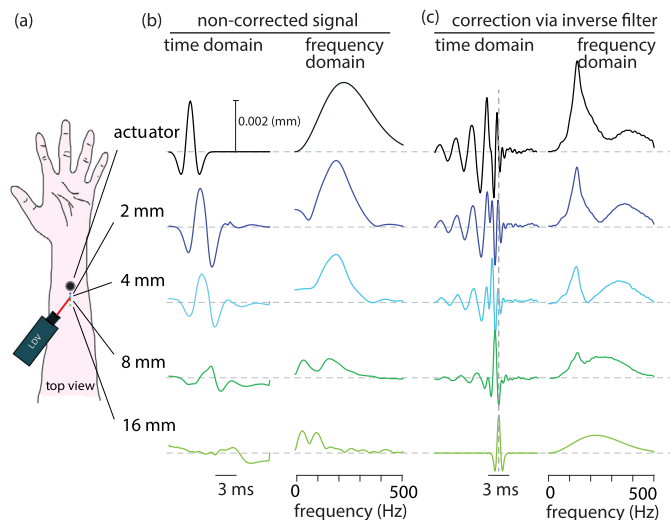
Fig. 4. Example of measured wave propagation with one actuator. (a) Schematic of the setup. (b) The non-corrected signal is generated by the actuators as a smooth and compact wavelet. During the propagation, the higher frequencies. (c) by sending the low frequencies first, the inverse filter focuses the energy into a compact wavelet at 16 mm.

measured on one actuator driven with the maximum amplitude of 10 V (see Fig. 4(b)).

4) Combination: The combination condition used the inverse filter method with the target displacement not equal to a Ricker wavelet but equal to the displacement signal produced by the funneling illusion condition. For a given participant, the target displacements at the location of the funneling illusion and the combination method were identical, while the driving signals differed. The driving signals for the combination method leveraged the knowledge of the viscoelastic properties of the participant's skin, while the funneling illusion did not account for the elastic property. This condition allowed us to verify whether manipulating the arrival time of the waves at the target location via phase, frequency, and amplitude control influenced our perception of localization.

D. Experimental Procedure

Before the experiments, the experimenter placed the wearable device on a participant such that each actuator made contact with the inner mid-side of their lower left arm, and velcro straps exerted 1 N force. Then the participant placed their arm on the foam in a comfortable pose by ensuring the square-shaped opening of the case was within the vibrometer field of view (see Fig. 2). We first measured the response of the skin to every actuator output. Once the calibration was done, we conducted two user studies.

1) Calibration: Before the calibration phase, the experimenter placed nine pieces of retro-reflective tape making a 3×3 array on the participant's skin within the case opening.

A transparent foil was covered on top of the squared-shaped case opening when all the driving signals were computed according to Fig. 3(a). A 3×3 grid was printed on the foil containing the nine grid numbers.

2) User Study 1: Performance: The first experiment aimed at gauging the localization performance of the participants for

the vibration stimuli was designed via three different stimulation methodologies. The participant's task was to identify where they felt the vibration stimulus most intense among the nine grid points indicated on their arm.

Each trial started with a brief beep sound cued via the headphones, while shortly after, a participant received a stimulus designed as focused at a randomly-selected grid point. Then, the participant entered a grid number of their choice using a numeric keyboard. For each participant, this experiment contained 81 (3 methodology $\times$ 9 grid location $\times$ 3 repetition) trials. Before starting the main session, each participant completed a training session identical to the main experiment but with five example trials.

3) User Study 2: Confidence: This study examined the confidence level of participants for localizing a propagated vibrotactile stimulus on the forearm. We used the same hardware set-up and experimental procedure as user study 1. However, in this case, participants could select more than one grid point if they could not identify a single location for the perceived stimulus. Before starting the main session, each participant completed a training session identical to the main experiment but with five example trials.

III. RESULTS

A. Wave Propagation

To estimate the frequency dependence of the wave speed and attenuation we ran a test with only one actuator and four aligned measurement points. The results of the propagation and decay can be found Fig. 4. At the location of the actuator, the waveform matches the Ricker wavelet, which spectrum spreads over a wide frequency range. As the wave packet travels down the arm, the waveform becomes more and more distorted, due to the non-uniform attenuation, which attenuated high-frequencies more strongly and due to a dispersion causing low frequency to travel slower through the medium.

When we apply the inverse filter to the case of a single actuator, we can correct the non-uniformity of the wave speed and wave attenuation to produce a wavelet at the furthest distance of 16 mm, see Fig. 4(b). To achieve this localization in space and time, the actuator generates a signal that resembles a chirp. The signal starts with low-frequency content and the high frequencies are amplified. Because the signal corrects for the medium acoustic behavior, the chirp collapses into a nicely formed wavelet.

A similar focusing is achieved when multiple actuators are driven in unison using the inverse method. Fig. 5 shows the results of focusing a Ricker wavelet at the center of four actuators placed at the corner. The displacement of the center point is faithful to the commanded displacement. The other points show some displacements but with lower amplitude than the center point.

B. User Study 1: Performance

Fig. 6 shows for each of the nine targets, the perceived sensation per localization technique for all 20 participants. The target locations are represented by the red stars and can be denoted
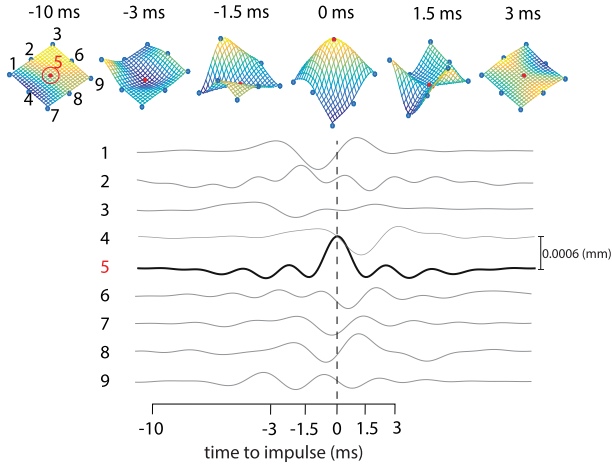
Fig. 5. Example of measured wave propagation using the inverse filter with multi actuators when focusing at the location 5. The top row shows the deformation at fixed instants. The bottom graph shows the time evolution of the displacement of all points. The deformation of point 5 is close to the Ricker wavelet used as input.
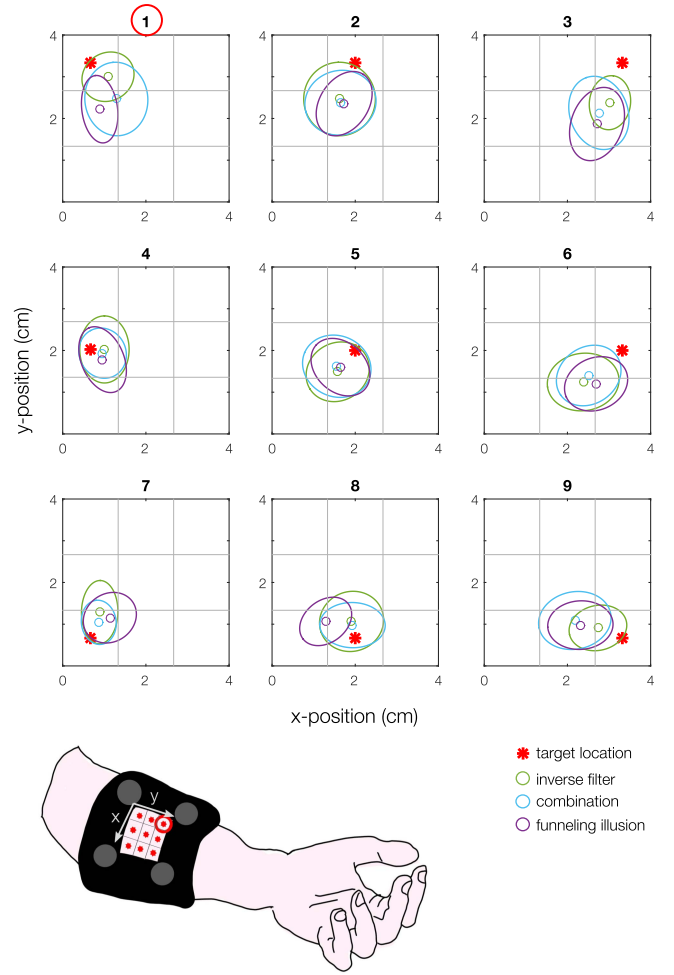

Fig. 6. Results of the user study 1. The calculated localization precision and accuracy are shown for each localization technique (inverse filter, combination, and funneling illusion) per target location (1–9). The red stars represent the target locations, whereas the three other color-coded circles indicate the mean position of the tactile sensation perceived by all participants for each technique. The ellipses around the mean show the accuracy of the perceived vibration. In the top left corner, a red circle is highlighted on target location 1, which represents the location of the red circle in the visualization of the set-up at the bottom of this figure.

by (x_i^t, y_i^t), where i stands for one out of the 9 locations on the 3×3 grid. The perceived locations (x_i^p, y_i^p) are displayed by 2D Gaussian distributions $N_i(\mu_i, \Sigma_i)$. Here μ_i describes the mean of the perceived location for all participants and Σ_i is the covariance matrix. The latter consists of a 2-by-2 matrix giving the auto-covariance of (x_i^p, x_i^p) and (y_i^p, y_i^p) on the diagonal axes and the cross-covariance (x_i^p, y_i^p) on the off-diagonal terms in the matrix. The covariance matrix is plotted as an ellipse at one standard deviation centered around the mean. Where the mean represents the accuracy, the covariance is a measure to show the precision.

Then, we examined the effects of target location and localization technique on the calculated error between the target and the perceived vibration [8] using the Euclidean distance:

$$e_{tot} = \sqrt{(x_i^p - x_i^t)^2 + (y_i^p - y_i^t)^2} \qquad (8)$$

Per target location and localization technique, 60 Euclidean distances (3 repetitions × 20 participants) were obtained. Then, we averaged the distances calculated for each participant for each condition. Afterward, we confirmed that the distributions passed the normality assumption via the Shapiro-Wilk test, and then we conducted two-way ANOVA with repeated measures. Mauchly's sphericity test showed that location failed this assumption; therefore, the F-value for this effect was corrected with Greenhouse-Geisser.

The results revealed that the target location had a statistically significant effect on the error ($F_{4.337,82.411} = 10.958$, $p < 0.0001$). This result can also be seen in Fig. 6, where the lower-left corner (4, 5, 7, and 8) outperformed the other target locations in the grid. Here the means of all the perceived vibrations are accumulated inside the targeted grid, whereas this observation does not hold for the other five locations.

Furthermore, our analysis showed that the localization technique also had a statistically significant effect on the error ($F_{2,38} = 6.090$, $p = 0.005$). A post hoc, paired t-test with a

Bonferroni correction found that there was only a significant difference between the classic funneling illusion and inverse filter ($p = 0.007$).

Moreover, there was a statistically significant interaction between the effects of location and localization technique on the error ($F_{16,304} = 3.919$, $p < 0.0001$). A post hoc, paired t-test with a Bonferroni correction indicated a statistically significant difference for 3 out of the 9 locations (1, 3, 9). We found that for these three locations, there were significant differences between the inverse filter and the other two techniques.

C. User Study 2 - Confidence

We examined the effects of location and localization techniques on the number of selected grid points. We first averaged the number of grid points given by each participant for each experimental condition. Then, the Shapiro-Wilk test revealed
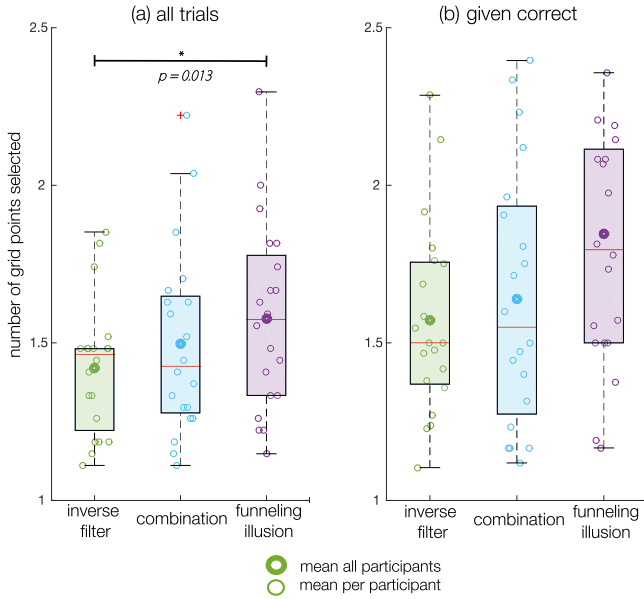
Fig. 7.   Results of user study 2. Box plots of the average number of selected grid points (a) from all trials, (b) from the trials where the perceived grid area was located within the correct target.

that the distributions failed the normality test. Therefore, we analyzed the results via a nonparametric Friedman test.

The results showed that location had a significant effect on the number of selected grid points ($\chi^2(8) = 30.749$, $p < 0.001$). Nonetheless, a post hoc, Bonferroni-corrected pairwise Wilcoxon test revealed that only locations 1 and 5 had a weak significant difference ($p = 0.46$).

Moreover, the effect of the localization technique was also found significant in the number of selected grid points ($\chi^2(2) = 15.797$, $p < 0.001$). A post hoc, Bonferroni-corrected pairwise Wilcoxon test showed that participants selected a significantly lower number of grid points with inverse filtering than with the funneling illusion ($p = 0.013$). The results indicate that participants had more confidence in localizing vibrotactile stimuli when presented with the inverse filter technique; compare the box plots for each methodology in Fig. 7. When the same analysis was conducted on only the trials where the perceived grid area was located within the correct target, the main effects (location and localization technique) were not found to be significant.

IV. DISCUSSION

In this article, we investigated whether the perceived localization of a stimulus created by funneling illusion on the skin can be improved by implementing an inverse filter. We hypothesized that since the inverse filter considers the dispersion and attenuation of the wave propagation on the skin, the resulting signal would lead to better-focused waves than the classic funneling technique, improving the perceived localization performance and confidence.

The skin vibration measurements illustrated that the inverse filter could successfully create a desired focused wave (e.g.,

Ricker wavelet) onto a target skin location while actively canceling the displacement as much as possible at the remaining positions (see Fig. 5). Nonetheless, when the desired signal was directly sent to the actuator without any correction, a dispersed wave occurred at the target location (compare Fig. 4(b) and (c). This dispersion is expected as waves decay through distance, and their propagation speed is frequency-dependent [24], [25].

Despite the well-focused wave, the localization performance of the participants did not show significant improvement with the inverse filter for most of the sites; the improvement was visible for only three corner points (see Fig. 6). This result supports the previous findings that suggested the funneling illusion is coded centrally [16], [17], and the peripheral factors have little effect on the localization performance. The performance difference for corner locations could be explained by the structure of the wearable device. In our design, the inner diameter of the device was the same over the entire length. However, the diameter of the forearm is not constant and decreases closer to the wrist. Hence, the two actuators next to locations 1 and 3 were partially in contact with the skin for most participants. Although the inverse filter technique considers this error in the calibration matrix $\mathbf{H}(\omega)$, the funneling illusion does not.

Nonetheless, the poor improvement in localization performance with inverse filter could also be explained by other factors, such as limitations of the experimental design and the applied body location. For example, the grid for the perceptual task had a small range, which covered only a limited area between the actuators, and low resolution, potentially have caused a bias towards the grid center. In addition, as the volar surface of the forearm is quite stiff [26] and the selected range is narrow, the correction of the inverse filter for the skin viscoelasticity to create a focused stimulus may not be more significant than the funneling illusion. It is possible that repetition of the same study with a grid having a larger range and resolution on a different body location with softer skin could reveal more drastic differences between the techniques. Finally, one might also investigate using the time reversal technique to improve the focus of the stimuli. This methodology showed promising results for providing localized tactile feedback on a soft surface [27].

Our findings indicated that the overall confidence for localizing illusionary stimuli improved significantly with the inverse filter although the given answers were not always located within the selected area; see Fig. 7(a). Therefore, focusing waves on the skin surface could possibly help participants to localize the illusionary stimulus within the limits of tactile sensitivity of the skin. In fact, earlier research by Cholewiak et al. [28] compared the localization performance on the entire arm and found that the middle of the forearm is not a reliable source for static localization. They showed that localization improved towards the anatomical landmarks such as the wrist and elbow, possibly caused by the higher tactile density of mechanoreceptors in these locations. Hence, the localization performance with the inverse filter could be improved for the body parts with a higher density of fast-adapting mechanoreceptors.

To the best of our knowledge, this is the first study that used focused acoustic waves on the skin via the inverse filter to create a localized vibrotactile sensation. Our results demonstrated that

the inverse filter could constructively focus surface waves toward a target location on the arm where no physical actuator is present. Whereas the overall ability to pinpoint where in the grid the participants perceived the vibration signal was not improved with the inverse filter technique for all the tested locations, confidence did improve significantly. These results suggest that the inverse filter can create localized and consistent stimuli across different participants within the limits of tactile sensitivity of the skin. Our findings can benefit industries interested in including localized vibrotactile feedback on the human body surface, such as the gaming, rehabilitation, and sports industry.

ACKNOWLEDGMENT

REFERENCES

[1] S. Fani et al., "Simplifying telerobotics: Wearability and teleimpedance improves human-robot interactions in teleoperation," *IEEE Robot. Automat. Mag.*, vol. 25, no. 1, pp. 77–88, Mar. 2018.

[2] J. G. Wildenbeest, D. A. Abbink, C. J. Heemskerk, F. C. van der Helm, and H. Boessenkool, "The impact of haptic feedback quality on the performance of teleoperated assembly tasks," *IEEE Trans. Haptics*, vol. 6, no. 2, pp. 242–252, Apr.–Jun. 2013.

[3] E. Pezent et al., "Explorations of wrist haptic feedback for AR/VR interactions with Tasbi," in *Proc. Adjunct Pub. 35th Annu. ACM Symp. User Interface Softw. Technol.*, 2022, pp. 1–5.

[4] C. Pacchierotti, S. Sinclair, M. Solazzi, A. Frisoli, V. Hayward, and D. Prattichizzo, "Wearable haptic systems for the fingertip and the hand: Taxonomy, review, and perspectives," *IEEE Trans. Haptics*, vol. 10, no. 4, pp. 580–600, Oct.–Dec. 2017.

[5] G. v. Békésy, "Funneling in the nervous system and its role in loudness and sensation intensity on the skin," *J. Acoustical Soc. Amer.*, vol. 30, no. 5, pp. 399–412, 1958.

[6] G. von Békésy, "Neural funneling along the skin and between the inner and outer hair cells of the cochlea," *J. Acoustical Soc. Amer.*, vol. 31, no. 9, pp. 1236–1249, 1959.

[7] O. B. Kaul, M. Rohs, B. Simon, K. C. Demir, and K. Ferry, "Vibrotactile funneling illusion and localization performance on the head," in *Proc. CHI Conf. Hum. Factors Comput. Syst.*, 2020, pp. 1–13.

[8] G. Park and S. Choi, "Tactile information transmission by 2D stationary phantom sensations," in *Proc. Conf. Hum. Factors Comput. Syst. - Proc.*, 2018, pp. 1–12.

[9] C. C. Berger and M. Gonzalez-Franco, "Expanding the sense of touch outside the body," in *Proc. 15th ACM Symp. Appl. Percep.*, 2018, pp. 1–9.

[10] D. S. Alles, "Information transmission by phantom sensations," *IEEE Tans. Man-Mach. Syst.*, vol. 11, no. 1, pp. 85–91, Mar. 1970.

[11] S.-Y. Kim and J. C. Kim, "Vibrotactile rendering for a traveling vibrotactile wave based on a haptic processor," *IEEE Trans. Haptics*, vol. 5, no. 1, pp. 14–20, Jan.–Mar. 2012.

[12] A. Israr and I. Poupyrev, "Tactile Brush: Drawing on skin with a tactile grid display," in *Proc. Conf. Hum. Factors Comput. Syst.- Proc.*, 2011, pp. 2019–2028.

[13] T. G. Sato, M. Ohsuga, H. Boutani, and T. Moriya, "Tactile phantom sensation for coaching respiration timing," *IEEE Trans. Haptics*, vol. 8, no. 1, pp. 119–125, Jan.–Mar. 2015.

[14] J. Salazar, K. Okabe, and Y. Hirata, "Path-following guidance using phantom sensation based vibrotactile cues around the wrist," *IEEE Robot. Automat. Lett.*, vol. 3, no. 3, pp. 2485–2492, Jul. 2018.

[15] A. Barghout, J. Cha, A. Saddik, J. Kammerl, and E. Steinbach, "Spatial resolution of vibrotactile perception on the human forearm when exploiting funneling illusion," in *Proc. IEEE Int. Workshop Haptic Audio Vis. Environ. Games*, 2009, pp. 19–23.

[16] E. P. Gardner and W. A. Spencer, "Sensory funneling. I. Psychophysical observations of human subjects and responses of cutaneous mechanoreceptive afferents in the cat to patterned skin stimuli," *J. Neurophysiol.*, vol. 35, no. 6, pp. 925–953, 1972.

[17] L. M. Chen, R. M. Friedman, and A. W. Roe, "Optical imaging of a tactile illusion in area 3b of the primary somatosensory cortex," *Science*, vol. 302, no. 5646, pp. 881–885, 1970.

[18] C. Hudin and S. Panëels, "Localisation of vibrotactile stimuli with spatio-temporal inverse filtering," in *Haptics: Science, Technology, and Applications*. Cham, Switzerland: Springer, 2018, pp. 338–350.

[19] L. A. Jones and N. B. Sarter, "Tactile displays: Guidance for their design and application," *Hum. Factors*, vol. 50, no. 1, pp. 90–111, 2008.

[20] S. Lederman and L. Jones, "Tactile and haptic illusions," *IEEE Trans. Haptics*, vol. 4, no. 4, pp. 273–294, Oct.–Dec. 2011.

[21] J. Seo and S. Choi, "Initial study for creating linearly moving vibrotactile sensation on mobile device," in *Proc. IEEE Haptics Symp.*, 2010, pp. 67–70.

[22] M. Tanter, J.-F. Aubry, J. Gerber, J.-L. Thomas, and M. Fink, "Optimal focusing by spatio-temporal inverse filter. I. Basic principles," *J. Acoustical Soc. Amer.*, vol. 110, no. 1, pp. 37–47, 2001.

[23] C. Hudin and L. Pantera, "Sparse actuator array combined with inverse filter for multitouch vibrotactile stimulation," in *Proc. IEEE World Haptics Conf.*, 2019, pp. 19–24.

[24] G. v. Békésy, "Human skin perception of traveling waves similar to those on the cochlea," *J. Acoustical Soc. Amer.*, vol. 27, no. 5, pp. 830–841, 1955.

[25] B. Dandu, Y. Shao, A. Stanley, and Y. Visell, "Spatiotemporal haptic effects from a single actuator via spectral control of cutaneous wave propagation," in *Proc. IEEE World Haptics Conf.*, 2019, pp. 425–430.

[26] M. Griffin, B. C. Leung, Y. Premakumar, M. Szarko, and P. E. Butler, "Comparison of the mechanical properties of different skin sites for auricular and nasal reconstruction," *J. Otolaryngol. - Head Neck Surg.*, vol. 46, 2017, Art. no. 33.

[27] G. Reardon, N. Kastor, Y. Shao, and Y. Visell, "Elastowave: Localized tactile feedback in a soft haptic interface via focused elastic waves," in *Proc. IEEE Haptics Symp.*, 2020, pp. 7–14.

[28] R. W. Cholewiak and A. A. Collins, "Vibrotactile localization on the arm: Effects of place, space, and age," *Percep. Psychophys.*, vol. 65, no. 7, pp. 1058–1077, 2003.